JOURNAL OF SOLID STATE CHEMISTRY 106, 310–316 (1993)

# The Pyroborate Fluoride $Ba_5(B_2O_5)_2F_2$

THEODORE ALEKEL III AND DOUGLAS A. KESZLER

*Department of Chemistry and Center for Advanced Materials Research, Oregon State University, Gilbert Hall (153), Corvallis, Oregon 97331-4003*

Received September 30, 1992; in revised form February 2, 1993; accepted February 4, 1993

The new material $Ba_5(B_2O_5)_2F_2$ represents the first confirmed structure of a pyroborate–halide anionic mixture in a crystalline phase. The structure contains four formula units in the monoclinic space group $C2/c$ (No. 15) with cell parameters $a = 20.726(3)$ Å, $b = 7.115(2)$, $c = 8.589(2)$, $\beta = 95.05(5)°$, and $V = 1261.7(5)$ Å$^3$. Its characterization reveals a three-dimensional structure of three face- and edge-sharing Ba-centered polyhedra that are also united through nonplanar pyroborate anions. These irregular polyhedra are eight- and nine-coordinate, and contain one or two F atom(s) at their peripheries. The geometry of the pyroborate is unusual in that the principal planes of the double triangles are rotated from one another by 86.6(1)°, the closest angular approach to the theoretical 90° limit of any known pyroborate; its B–O–B angle of 121.6(5)°, however, is typical. Differential thermal analysis reveals single events on heating and cooling that are indicative of a congruently melting compound.


## Introduction

With a dozen structures reported (*1–12*), pyroborates represent a very small, but growing, percentage of all the known borate compounds. The pyroborate group can be viewed as two orthoborate units that link together via a common O atom. Typically, as the boron concentration of a borate increases in composition with respect to the other cations present, the borate groups condense to form more complex polyatomic anions. $Sr_3(BO_3)_2$ (*13*) versus $Sr_2B_2O_5$ (*2*) exemplifies this trend: when the compositional B : Sr ratio (mol%) increases, the condensed borate arrangement is favored. Intermediately, between the exclusive formation of either orthoborate or pyroborate, the compounds $Sr_2Sc_2B_4O_{11}$ [$\equiv Sr_2Sc_2B_2O_5(BO_3)_2$] and $Ba_2Sc_2B_4O_{11}$ (*1*) incorporate *both* borate configurations within the same structure.

The compound $Ba_5(B_2O_5)_2F_2$ represents an additional example of a pyroborate containing a mixture of anions and, in fact, the first pyroborate halide structurally confirmed to exist. Two other pyroborate fluorides, $Al_2(B_2O_5)F_2$ (*14*) and $Sc_2(B_2O_5)F_2$ (*15*), have been proposed but their structural identity has not been verified. The title compound is also distinctive in that it is one of the first barium borate fluorides to be described (*16*). Even though a phase diagram for the binary system $BaF_2$–$B_2O_3$ has been proposed (*17*) and a barium fluoroborate, $BaBOF_3$, is purported to exist (*18*), our investigations indicate this phase system to be more complex than previously reported. In this paper we describe the structural and thermal properties of $Ba_5(B_2O_5)_2F_2$.

## Experimental

### *Synthesis*

The synthesis of $Ba_5(B_2O_5)_2F_2$ was achieved by a high-temperature solid-state reaction of high-purity reagents. Samples were obtained by melting a stoichiometric mixture of $BaCO_3$ (ÆSAR, 99.9%), $BaF_2$ (Alfa, optical grade), and $B_2O_3$ (Alfa, 99.98%) at 1175 K for 1 hr and allowing the material to cool to room temperature by

0022-4596/93 $5.00

turning off the furnace. Crystals were originally grown from a melt with the mol% ratio of 65.25 BaO : 24.87 $BaF_2$ : 9.88 $B_2O_3$; the title compound and the new material $Ba_7(BO_3)_3F_5$ coprecipitated from this melt. Their coexistence was confirmed by powder X-ray diffraction analysis. Experimental patterns were compared with calculated patterns that were generated with the program LAZY–PULVERIX (*19*). Upon discovering the true components in the mixture, a pure batch of clear pyroborate crystals was made by slowly cooling a stoichiometric ratio of the reagents.

### *Thermal Measurements*

To determine melting characteristics of the compound, differential thermal analysis (DTA) was performed. Measurements were made on a Harrop 726 differential thermal analyzer that had been interfaced to a personal computer through a Metrabyte M1531 resistance-to-voltage converter and a Real Time Devices AD100A analogue-to-digital converter. The system was calibrated with a pure gold reference, the samples (~5 mg) were held in Pt containers. The heating and cooling rates were ±20 K/min.

### *X-Ray Work*

A clear prismatic block of dimensions 0.09(1) × 0.12(1) × 0.22(1) mm was mounted on a glass fiber and analyzed on a Rigaku AFC6R single crystal X-ray diffractometer. Unit cell parameters were derived from a least-squares fit of 20 automatically centered setting angles within the angular range $30 < 2\theta < 36°$. Peaks were measured to a width of $1.50 + 0.30 \tan\theta$ by using $\omega$ scans at a rate of 16°($\omega$)/min. The stability of the crystal was confirmed by the constancy of three standards measured every 300 reflections, so no decay correction was implemented. From 2032 reflections measured to $2\theta = 60°$ with Miller index limits $0 \le h \le 30$; $0 \le k \le 10$; $-12 \le l \le 12$, 1661 data were found to have $F_0^2 > 3\sigma(F_0^2)$.

TABLE I

CRYSTALLOGRAPHIC DATA

| | |
|---|---|
| Chemical formula | $Ba_5(B_2O_5)_2F_2$ |
| Formula weight (amu) | 965.88 |
| Space group | $C2/c$ (No. 15) |
| $a$ (Å) | 20.726(3) |
| $b$ (Å) | 7.115(2) |
| $c$ (Å) | 8.589(2) |
| $\beta$ (°) | 95.05(5) |
| $V$ (Å$^3$) | 1261.7(5) |
| $Z$ | 4 |
| $\rho_{calc}$ (g cm$^{-3}$) | 5.084 |
| $\mu$ (cm$^{-1}$) | 154.82 |
| Transmission factors | 0.83–1.23 |
| Diffractometer | Rigaku AFC6R |
| Radiation | Mo $K\alpha^a$ |
| $T$ (K) | 300 |
| Data collection | $h, k, \pm l$ |
| No. of observations | 4144 |
| $R, R_w{}^b$ | 0.043, 0.058 |

[a] Graphite monochromated, $\lambda = 0.71069$ Å

[b] $R = \Sigma\,||F_0| - |F_c||/\Sigma\,|F_0|$, $R_w = \sqrt{\Sigma\, w(|F_0| - |F_c|)^2/\Sigma\, w|F_0|^2}$.

General crystallographic information is summarized in Table I.

Data analysis was performed on a Digital $\mu$VAX II computer, and the crystal structure was determined by using the TEXSAN crystallographic software package (*20*). The systematic absences $h0l$: $l = 2n + 1$ and $00l$: $l = 2n + 1$ are consistent with the monoclinic space groups $C2/c$ and $Cc$. On the basis of the statistical distribution of intensities (*21*) and the successful solution, we favor the centrosymmetric group $C2/c$.

The Ba atoms were located with the direct methods program SHELXS-86 (*22*), and the remaining atoms were found by subsequent analysis of an electron density map. The values of $F_{calc}$ were derived from predetermined neutral scattering factors and adjusted for anomalous dispersion by using $f'$ and $f''$ factors from the "International Tables of X-ray Crystallography (Vol. IV, 1974)." Following refinement with isotropic displacement coefficients on each atom, the data were corrected for absorption with the program DIFABS (*23*) and subsequently averaged ($R_{int} = 0.064$). All atoms were

TABLE II

ATOMIC COORDINATES AND THERMAL DISPLACEMENT COEFFICIENTS

| | $x$ | $y$ | $z$ | $B_{eq}$ (Å$^2$)[a] |
|---|---|---|---|---|
| Ba1 | 0.30022(2) | 0.11327(5) | 0.69253(4) | 0.95(1) |
| Ba2 | 0.08508(2) | 0.11605(5) | 0.60801(4) | 1.00(1) |
| Ba3 | 0 | 0.44454(8) | ¼ | 1.03(2) |
| F | 0.4204(3) | 0.3262(7) | 0.6960(5) | 1.6(2) |
| O1 | 0.4036(3) | −0.0002(8) | 0.9599(7) | 1.6(2) |
| O2 | 0.3494(2) | 0.2968(8) | 0.9632(7) | 1.2(1) |
| O3 | 0.2196(3) | −0.0318(7) | 0.9419(6) | 1.5(2) |
| O4 | 0.3127(3) | −0.2628(8) | 0.7152(5) | 1.2(1) |
| O5 | 0.0413(3) | 0.2350(9) | 0.9216(7) | 1.6(2) |
| B1 | 0.4057(3) | 0.180(1) | 0.0051(8) | 0.9(2) |
| B2 | 0.1890(3) | 0.131(1) | 0.9180(8) | 0.9(2) |

[a] $B_{eq} = (8\pi^2/3)\,\Sigma_i\,\Sigma_j\,U_{ij}a_i^*a_j^*\mathbf{a}_i\cdot\mathbf{a}_j$

then refined with anisotropic displacement parameters. Least-squares convergence ($\Delta/\sigma < 0.01$) with a secondary extinction coefficient = $0.9(3) \times 10^{-6}$ affords the residuals $R = 0.043$ and $R_w = 0.058$, where $\sigma(F^2) = [C + \frac{1}{4}(t_c/t_b)^2(b_1 + b_2) + (pI)^2]^{1/2}$ and $p = 0.03$. The maximum peak in the final difference electron density map of 1.905 $e$ Å$^{-3}$ amounts to 0.80% of the Ba1 atom, and the minimum peak is $-2.237$ $e$ Å$^{-3}$. Atomic positions and equivalent isotropic displacement coefficients are listed in Table II.

## Results

### *Structure Description*

A labeled drawing of the unit-cell contents is given in Fig. 1 for atomic identification purposes. To discern the connectivity within the cell, the stereo drawing of Fig. 2 provides a more suitable view. $Ba_5(B_2O_5)_2F_2$ forms a three-dimensional framework of face- and edge-sharing Ba-centered polyhedra that are interconnected through nonplanar pyroborate units. Although the overall arrangement is not layered, each of the three Ba types exclusively resides on a *bc* plane, repeating along the *a* axis as Ba3–Ba2–Ba1–Ba1–Ba2 strata. The $F^-$ and $(B_2O_5)^{4-}$ anions contribute to linking these $Ba^{2+}$ cations in all directions and establishing the full three-dimensional structure.

In considering the nature of each Ba site, we see that the Ba1 atom has a unique coordination environment in comparison with the other two types. It is surrounded by eight O atoms and one F atom at the vertices of an irregular *s*-tricapped trigonal prism. On the other hand, the Ba2 and Ba3 atoms are octacoordinate (distorted undecahedra and bicapped trigonal prisms—capping on one square face—respectively), each bonding to eight O atoms and two F atoms. Since the Ba3 atom is the only one that rests on

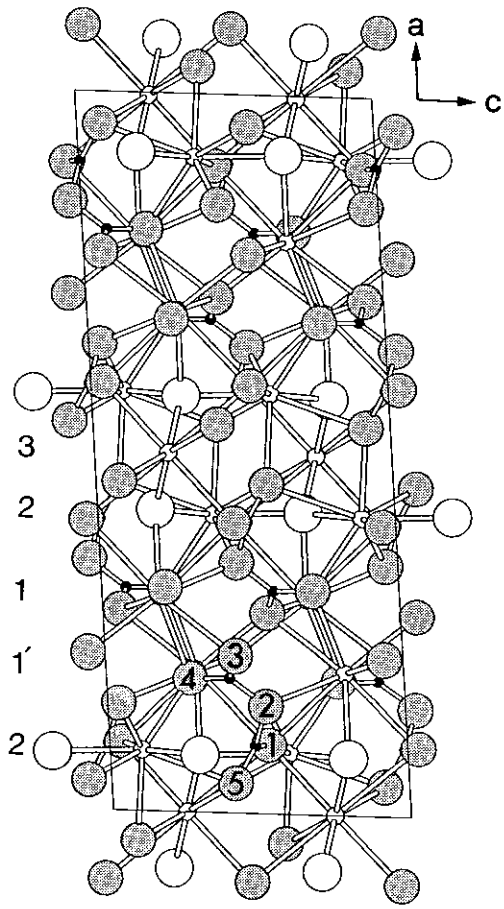


FIG. 1. A schematic unit cell drawing of $Ba_5(B_2O_5)_2F_2$ along the *b*-axis. The small open circles represent Ba atoms, the large shaded circles represent O atoms, the small black circles represent B atoms, and the large open circles represent F atoms. (Atomic legend continued for subsequent figures.) The Ba layers and the O atoms are numerically labelled.

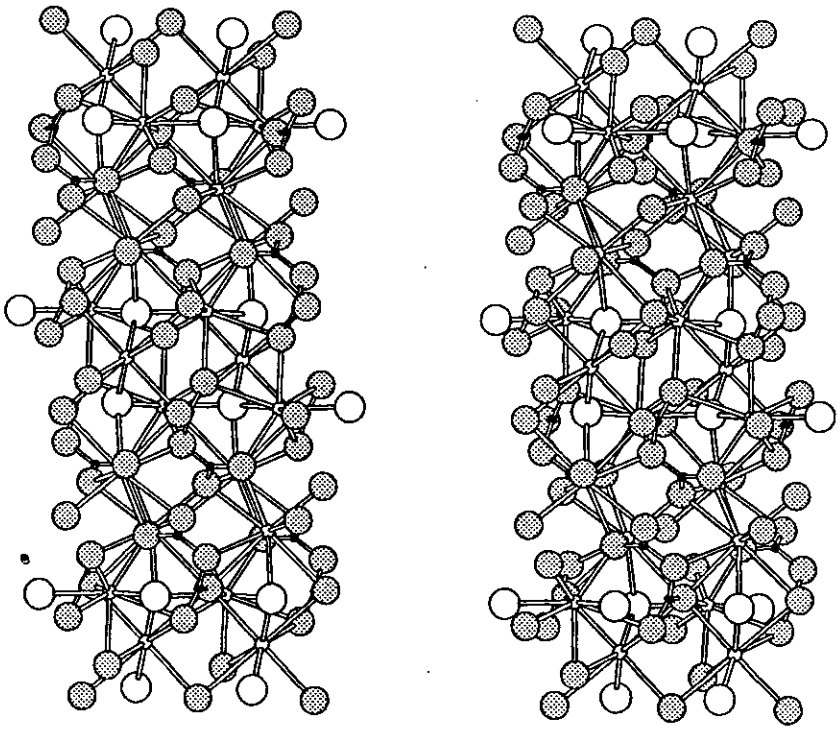

FIG. 2. A *b*-axis projected stereo view of the unit cell along the *b*-axis.

a special position in the cell, it alone possesses any symmetry ($C_2$) other than simple identity.

The connectivity within the structure is illustrated in Fig. 3 and is hereby described: The $Ba(1)O_8F$ polyhedra share common O··O edges with other Ba1 atoms in the same *bc* plane and additional O··O edges with Ba1 atoms (1′) that are located in an adjacent plane displaced along the **a** direction (Fig. 3a). Furthermore, they share O··O and O··F edges with $Ba(2)O_6F_2$ distorted undecahedra (cf. Figs. 2 and 3a) and adjoin to $Ba(3)O_6F_2$ bicapped trigonal prisms through common O··F··O faces (Fig. 3b). With respect to the pyroborate groups, each Ba1 environment shares two edges with $(B_2O_5)^{4-}$ anions, consisting of a bridging O atom ($O_b$) and a terminal O atom ($O_t$) of the pyroborate group. An additional edge of the Ba1-centered polyhedron spans two $O_t$ atoms, one from each $BO_2$ endmember, to establish an O1–B1–O2–B2–O4 bridge (Fig. 3b). The Ba2-centered distorted undecahedra also coordinate opposite ends of this pyroborate link by using the same $O(4)_t$ atom on one end and the complementary $O_t$ atom of the other $BO_2$ endmember, thus forming another bridge (O5–B1–O2–B2–O4) to a single Ba center. The $Ba(2)O_6F_2$ undecahedra are connected to each other via O··F edges; additionally, they couple to $Ba(3)O_6F_2$ bicapped trigonal prisms through common O··O edges and shared triangular O faces. The prisms are joined to one another by common O··O edges, and they share edges and corners with the $O_t$ atoms of pyroborates.

Selected interatomic distances and angles are listed in Table III. Even though the average Ba–O lengths of 2.86(2) and 2.84(2) Å for the respective Ba1 and Ba2 polyhedra compare to the length 2.85 Å predicted from the radii (*24*), both sites exhibit a wide variation of values as indicated by the large standard deviation ±0.2 Å for each polyhedron

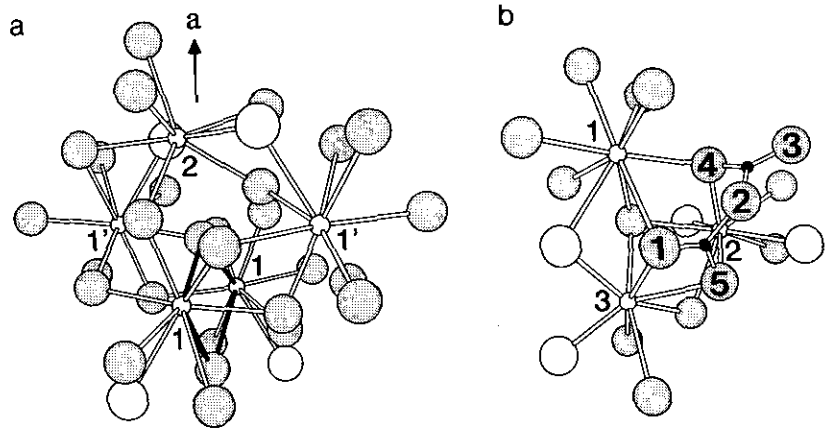


FIG. 3. Illustrations of the interconnectivity between selected polyhedra: (a) The shared edges between the coplanar Ba1 centers are highlighted as shaded bonds; the other layer is labeled Ba1'. (b) The pyroborate connectivity to the Ba polyhedra; the Ba atoms and the pyroborate O atoms are numerically labeled.

(cf. Table III). The Ba–F distances of 2.915(6) Å for Ba1, 2.673(5) and 2.633(5) Å for Ba2, and 2.552(5) Å (×2) for Ba3 illustrate the extensibility of these interactions from the calculated distance of 2.73 Å. As a result, the F atom is coordinated by four Ba atoms that form a distorted tetrahedron with an average Ba–F–Ba angle of 108.6(5)°. The symmetric $Ba(3)O_6F_2$ exhibits the shortest Ba–F interactions and considerable deviation from characteristic Ba–O interactions with a long average Ba3–O length of 2.91(2) Å.

The pyroborate group within $Ba_5(B_2O_5)_2F_2$ contains a spread of lengths between 1.32(1) and 1.46(1) Å, but the average of 1.38(2) Å equals the expected B–O distance of a tricoordinate B atom. The distribution of the individual interactions follows a common trend for pyroborates: the B1 and B2 atoms have a short and a normal distance to the $O_t$ atoms, while the interactions to the $O_b$ atom are both long. This observation compares to the B–O lengths in the pyroborates $BaCuB_2O_5$ (*3*) and $Sr_2ScLi(B_2O_5)_2$ (*4*) where the B–$O_b$ length equals 1.42(1) Å.

For the title compound, the $O_t$–B–$O_t$ angles for each B type is 5° wider than the regular trigonal angle of 120°, whereas the $O_t$–B–$O_b$ angles containing the bridging O2 atom are narrower than 120°. This imitates the expanded angles of the pyroborate $BO_2$ endmembers witnessed in the compounds $Sr_2Sc_2B_4O_{11}$ and $Ba_2Sc_2B_4O_{11}$ (*1*). These angular distortions appear to be dictated by the coordinative stricture of the bound metals; in both of these examples, the $O_t$–B–$O_t$ end-members bridge two individual metal centers, so this angle is largely determined by their separation within the structure. The expanded $O_t$–B–$O_t$ angles within $Ba_5(B_2O_5)_2F_2$, on the other hand, are multiply governed by edge-sharing Ba1- and Ba3-centered polyhedra and by bridging the three Ba centers together.

The parameters that describe the geometric attributes of the pyroborate group, namely the B–O–B angle and the *interplanar angle*, are depicted in Fig. 4. The interplanar angle is defined as the angle between the vectors normal to the end $B(O_t)_2$ planes. In the title structure, the B–$O_b$–B angle of 121.2(6)° is typical among pyroborate compounds (*5*, *6*) which can exhibit angular extremes that range from 111.8 to 180° (*7*, *1*). The notable feature of $Ba_5(B_2O_5)_2F_2$, however, is the interplanar angle of 86.6(1)° between the double triangles; it represents the current maximum twist angle witnessed in any known pyroborate (theo-

TABLE III

SELECTED BOND DISTANCES AND ANGLES

| | | | |
|---|---|---|---|
| Ba1–F | 2.915(6) | F–Ba1–O1 | 60.7(1) |
| Ba1–O1 | 3.110(6) | O1–Ba1–O1 | 86.5(2) |
| Ba1–O1 | 3.157(6) | O1–Ba1–O2 | 47.6(2) |
| Ba1–O2 | 2.791(5) | O2–Ba1–O3 | 75.5(2) |
| Ba1–O3 | 3.018(6) | O3–Ba1–O3 | 98.6(2) |
| Ba1–O3 | 2.668(6) | O3–Ba1–O3 | 78.8(2) |
| Ba1–O3 | 2.794(6) | O3–Ba1–O4 | 79.0(2) |
| Ba1–O4 | 2.682(6) | O4–Ba1–O4 | 112.6(2) |
| Ba1–O4 | 2.696(6) | O2–Ba1–O6 | 83.9(3) |
| Ba2–F | 2.673(5) | F–Ba2–F | 138.2(2) |
| Ba2–F | 2.633(5) | F–Ba2–O1 | 68.8(2) |
| Ba2–O1 | 2.808(6) | O1–Ba2–O2 | 134.7(2) |
| Ba2–O2 | 2.744(6) | O2–Ba2–O4 | 90.6(2) |
| Ba2–O4 | 2.643(6) | O4–Ba2–O5 | 71.7(2) |
| Ba2–O5 | 3.039(6) | O2–Ba2–O5 | 48.5(2) |
| Ba2–O5 | 3.064(6) | O5–Ba2–O5 | 68.8(2) |
| Ba2–O5 | 2.744(6) | F–Ba2–O5 | 68.0(2) |
| Ba3–F | 2.552(5) × 2 | F–Ba3–F | 82.0(3) |
| Ba3–O1 | 3.075(6) × 2 | O1–Ba3–O1 | 84.9(2) |
| Ba3–O1 | 2.838(6) × 2 | O1–Ba3–O1 | 93.1(2) |
| Ba3–O5 | 2.805(6) × 2 | O5–Ba3–O5 | 71.5(3) |
| B1–O1 | 1.33(1) | O1–B1–O2 | 118.6(8) |
| B1–O2 | 1.46(1) | O1–B1–O5 | 124.2(8) |
| B1–O5 | 1.36(1) | O2–B1–O5 | 116.9(7) |
| B2–O2 | 1.43(1) | O2–B2–O3 | 119.5(7) |
| B2–O3 | 1.32(1) | O2–B2–O4 | 114.6(7) |
| B2–O4 | 1.37(1) | O3–B2–O4 | 125.8(7) |

retical limit = 90°). The group in $Sr_2Sc_2B_4O_{11}$ illustrates the complementary configuration, possessing coplanar double triangles (0°). These interplanar limits and the variety of intermediate angles among other compounds are consistent with the absence of a significant energy barrier that might afford a favorable geometry. This result has also been noted from the results of extended Hückel calculations where the energy differences among various geometries was found to be trivial (*1*).

*Thermal Properties*

The data obtained from the DTA measurement reveal simple single events for the heating and cooling curves (Fig. 5). Upon heating, the sample melted at a temperature of 1040 K and exhibited no further evidence of decomposition or phase transformation. The baseline shift flanking the melting curve indicates a change in thermal conductivity of the solid versus the liquid. As the temperature is decreased, the melt supercools by approximately 150 K after passing through its freezing point.

Recall that the growth of the $Ba_5(B_2O_5)_2F_2$ crystals was achieved without the aid of a flux. This fact, along with the DTA findings, suggests that the title compound melts congruently. In addition, upon cycling the sample through the melting point several times, the same thermal response was recorded. If, on the other hand, the compound was incongruent, then decompositional phase changes would be evident, rendering the system irreversible when cycled. These results are consistent with the structural arrangement—all of the atoms are situated in favorable environments to form a thermodynamically stable compound from the melt composition. Evidence to support the ki-

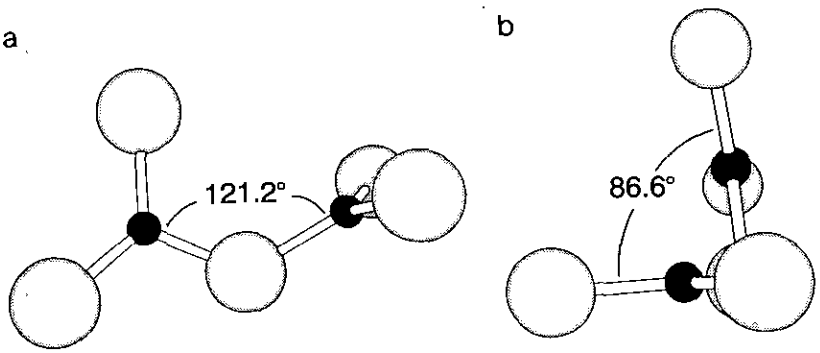


FIG. 4. The pyroborate geometry of $Ba_5(B_2O_5)_2F_2$: (a) the B–O–B angle and (b) the interplanar angle.

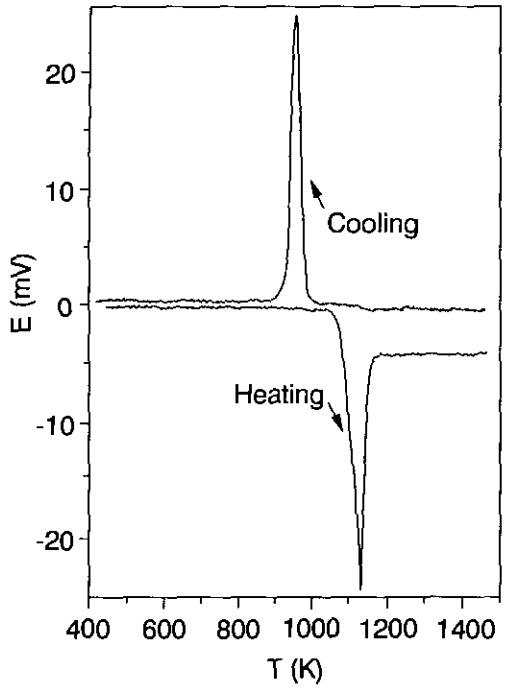


FIG. 5. DTA data for $Ba_5(B_2O_5)_2F_2$.

netic spontaneity of formation is again drawn from the nature of the synthesis procedure. The compound can be made in a matter of minutes by melting the starting materials and quenching the liquid to room temperature by directly removing the melt from the oven; powder X-ray diffraction confirms the immediate generation of $Ba_5(B_2O_5)_2F_2$ from this accelerated synthetic procedure. Therefore, the rapid nucleation and formation of crystals signify no practical kinetic barrier to crystallization—a surprising result considering that the compositional components are common glass formers.

## Acknowledgments

This research was supported by the US National Science Foundation, Solid-State Chemistry Program (DMR-8814432). Acknowledgment is made to the donors of The Petroleum Research Fund, administered by the American Chemical Society, for partial support of this research. DAK thanks the Alfred P. Sloan Research Foundation for a fellowship.

## References

1. P. D. THOMPSON, J. HUANG, R. W. SMITH, AND D. A. KESZLER, *J. Solid State Chem.* **95,** 126 (1991).
2. H. BARTL AND W. SCHUCKMANN, *Neues Jahrb. Min. Monatsh.* **8,** 253 (1966).
3. R. W. SMITH, Ph.D. dissertation, Oregon State University (1989).
4. P. D. THOMPSON AND D. A. KESZLER, *Solid State Ionics* **32/33,** 521 (1989).
5. O. V. YAKUBOVICH, M. A. SIMONOV, E. L. BELOKONEVA, Y. IC EGOROV-TISMENKO, AND N. V. BELOV, *Dokl. Akad. Nauk SSSR* **230,** 837 (1976).
6. O. V. YAKUBOVICH, N. A. YAMNOVA, B. M. SHCHEDRIN, M. A. SIMONOV, AND N. V. BELOV, *Dokl. Akad. Nauk SSSR* **228,** 842 (1976).
7. O. V. YAKUBOVICH, M. A. SIMONOV, AND N. V. BELOV, *Dokl. Akad. Nauk SSSR* **238,** 98 (1978).
8. Y. TAKÉUCHI, *Acta Crystallogr.* **5,** 574 (1952).
9. S. BLOCK, G. BURLEY, A. PERLOFF, AND R. D. MASON, *J. Res. Natl. Bureau Standards* **62,** 95 (1959).
10. S. BERGER, *Acta Chem. Scand.* **4,** 1054 (1950).
11. H. KÖNIG, R. HOPPE, AND M. JANSEN, *Z. Anorg. Allg. Chem.* **449,** 91 (1979).
12. M. GASPERIN, *Acta. Crystallogr. Sect. B* **30,** 1181 (1974).
13. L. RICHTER AND F. MÜLLER, *Z. Anorg. Allg. Chem.* **467,** 123 (1980).
14. K. TESKE AND H. A. LEHMANN, *Z. Chem.* **6,** 230 (1966).
15. L. R. BATSANOVA, L. A. NOVOSEL'TSEVA, AND A. I. MADARAS, *Inorg. Mater. (Engl. Transl.)* 530 (1974).
16. The other phase discovered in this system is $Ba_7(BO_3)_3F_5$. T. ALEKEL III, Ph.D. dissertation, Oregon State University (1993).
17. S. I. BERUL' AND I. N. NIKONOVA, *Russ. J. Inorg. Chem.* **11**(4), 490 (1966).
18. D. M. CHACKRABURTTY, *Acta Crystallogr.* **10,** 199 (1957).
19. K. YVON, W. JEITSCHKO, AND E. PARTHÉ, *J. Appl. Crystallogr.* **10,** 73 (1977).
20. Molecular Structure Corporation, "TEXSAN: Single Crystal Structure Analysis Software, Version 5.0," MSC, The Woodlands, TX (1985).
21. E. HOWELLS, D. PHILLIPS, AND D. RODGERS, *Acta Crystallogr.* **3,** 210 (1950).
22. G. M. SHELDRICK, SHELXS86, *in* "Crystallographic Computing 3" (G. M. Sheldrick, C. Krüger, and R. Goddard, Eds.), p. 175 Oxford Univ. Press, Oxford (1985).
23. N. WALKER AND D. STUART, *Acta Crystallogr. Sect. A* **39,** 158 (1983).
24. R. D. SHANNON, *Acta Crystallogr. Sect. A* **32,** 751 (1976).